



Published in final edited form as:

Nat Chem Biol. 2020 June ; 16(6): 695–701. doi:10.1038/s41589-020-0509-x.

Topology-Dependent Interference of Synthetic Gene Circuit Function by Growth Feedback

Rong Zhang^{1,#}, Jiao Li^{1,2,#}, Juan Melendez-Alvarez¹, Xingwen Chen¹, Patrick Sochor¹, Hanah Goetz¹, Qi Zhang¹, Tian Ding², Xiao Wang^{1,*}, Xiao-Jun Tian^{1,*}

¹School of Biological and Health Systems Engineering, Arizona State University, Tempe, Arizona, USA.

²Department of Food Science and Nutrition, Zhejiang University, Hangzhou, Zhejiang, China.

Abstract

Growth-mediated feedback between synthetic gene circuits and host organisms leads to diverse emerged behaviors, including growth bistability and enhanced ultrasensitivity. However, the range of possible impacts of growth feedback on gene circuits remains underexplored. Here, we mathematically and experimentally demonstrated that growth feedback affects the functions of memory circuits in a network topology-dependent way. Specifically, the memory of the self-activation switch is quickly lost due to the growth-mediated dilution of the circuit products. Decoupling of growth feedback reveals its memory, manifested by its hysteresis property across a broad range of inducer concentration. On the contrary, the toggle switch is more refractory to growth-mediated dilution and can retrieve its memory after the fast-growth phase. The underlying principle lies in the different dependence of active and repressive regulations in these circuits on the growth-mediated dilution. Our results unveil the topology-dependent mechanism on how growth-mediated feedback influences the behaviors of gene circuits.

INTRODUCTION

Circuit-host interactions affect behaviors of synthetic gene circuits, thereby adding an additional layer of complexity to already intricate gene regulatory networks^{1–3}. There are many sources of circuit-host interactions, including metabolic burden^{4,5}, cell growth^{6–8}, and

Users may view, print, copy, and download text and data-mine the content in such documents, for the purposes of academic research, subject always to the full Conditions of use:http://www.nature.com/authors/editorial_policies/license.html#terms

* xiaojun.tian@asu.edu, xiaowang@asu.edu.

#These authors contributed equally to this work: Rong Zhang, Jiao Li

Author Contributions

X-J.T. conceived the study. X-J.T., R.Z., and X.W. designed the study. R.Z., J.L., P.S., and X.C. performed experiments. J.M-A., H.G., and X-J.T. performed model studies. R.Z., X-J.T., Q.Z., T.D., and X.W. analyzed the data. R.Z. and X-J.T. wrote the manuscript. H.G. and X.W. edited the manuscript.

Conflict of Interest

The authors declare no competing financial interests.

Data availability.

All data produced or analyzed for this study are included in the published article and its supplementary information files or are available from the corresponding author upon reasonable request.

Code availability.

All the equations and parameters of the mathematical models can be found in the supplementary note.

resource relocation/competition^{9–12}. These interactions are often neglected in the design of gene circuits by assuming that gene circuits are generally orthogonal to the host background^{13–16}. In many instances, however, the impacts of circuit-host interactions are significant^{17–19}. Understanding the mechanisms of how circuit-host interactions are established, particularly the effects of these interactions on gene circuit functions, will help us to better formulate control strategies for designing and engineering robust gene circuits.

Various feedback loops are created by circuit-host interactions. For example, growth feedback is formed given that the expression of synthetic gene circuits inevitably causes metabolic burden to host cells and thus affects cell growth, which in turn changes gene expression of circuits^{8,20}. This growth feedback endows gene circuits with various emerged properties, including enhanced ultrasensitivity^{21,22}, innate growth bistability²³, and toxin cooperativity²⁴. However, the desired functions of gene circuits also can be attenuated by growth feedback.

Here, we studied how the network topology affects the extent to which growth feedback influences the memory maintenance function of synthetic switch circuits. Several different topologies can be used to create a bistable switch, including toggle switch or self-activation (SA) switch^{25–31}. Previously, it was theoretically predicted that self-activation or toggle switch would be differently regulated by growth feedback under constant growth rate conditions^{8,20}. To test the hysteresis properties of these switches, one dilution protocol was often used to ensure cells in the exponential growth phase. For example, in the seminal work of the toggle switch, all the samples were diluted in fresh medium every 6–10 hours²⁵. The underlying reason is that cell growth can be maintained at a relatively constant rate. While this dilution protocol works successfully to demonstrate the hysteresis behavior, an important question naturally arises concerning whether bistable behavior can be observed robustly in conditions where the growth rate is rather dynamic instead.

Here, we systematically tested the dynamics of two bistable switches under various cell growth conditions. We found that the memory of the self-activation switch is lost due to cell growth, and thus no hysteresis was found using the dilution protocol with fresh medium. However, after uncoupling growth feedback from gene circuits, we found a broad range of bistability. On the contrary, the toggle switch is more refractory to growth feedback. We demonstrated this underlying mechanism using mathematical modeling and theoretical analysis by integrating the dynamics of cell growth into the gene circuits. Thus, we concluded that the effects of growth-mediated feedback on gene circuits depend on their network topologies.

RESULTS

Inconsistent *in silico* and *in vivo* analysis of SA circuit

To determine the effects of growth feedback on gene circuits, we first built a simple SA circuit, in which the transcriptional factor AraC forms a dimer and binds to promoter P_{BAD} in the presence of stimulus L-(+)-arabinose (L-ara), which in turn activates the expression of itself and the reporter green fluorescent protein (GFP). We measured the dose-response curve of promoter P_{BAD} , which shows ultrasensitivity after parameter fitting (Fig. 1a). Based

on the fitted parameters, we developed a mathematical model for the SA circuit (see supplementary note for details) and predicted that the SA circuit is bistable. As shown in Fig. 1b, the system switches from 'OFF' to 'ON' once the stimulus level reaches above the threshold and stays in the 'ON' state even if the stimulus is removed.

To test our prediction, we measured the response of the SA circuit with varying doses of L-ara. Clear bimodal distributions were observed in a broad range of L-ara concentrations (Fig. 1c), with some cells in a GFP^{high} state and others in a GFP^{low} state, suggesting the system could be bistable. Further experiments were conducted to test the hysteresis behavior. First, initially 'OFF' cells were treated with a series dose of L-ara for 17 hours, and the fraction of 'ON' cells was measured by flow cytometry above, which shows a switch behavior (Fig. 1d, black line). Second, 'ON' cells (pretreated with high-dose L-ara) were diluted into fresh medium with various concentrations of L-ara. After 18 hours, the 'ON' cells fraction showed a curve similar to the one without pretreatment (Fig. 1d, red line), which was confirmed by the similar steady-state GFP curves (Supplementary Fig. 1). Thus, seemingly inconsistent conclusions are drawn between theoretical prediction and experimental verification.

Growth feedback disguises bistability of SA circuit

To uncover the underlying reason for this inconsistency, we further studied the temporal dynamics of activated cells. After diluting the activated cells into fresh media with various concentrations of L-ara, the cell density (measured as optical density, OD at 600 nm) and GFP fluorescence were measured at different time points. We observed that cell growth slowed as the population reached the carrying capacity, following the logistic model (Fig. 2a). However, the average GFP level (GFP/OD) decreased rapidly during the exponential growth phase and reached a very low level 3 hours after dilution (Fig. 2b), indicating the memory loss of the circuit. Later, GFP started accumulating and then reached different steady states depending on L-ara levels (Fig. 2b) and generated curves similar to the ones started from the inactive state (Supplementary Fig. 2). It is important to note that the GFP level maintained very well for 6 hours after the cells reached the stationary phase. To exclude potential factors associated with the stationary phase for memory loss, cells activated by high dose of L-ara to different levels of GFP at different OD (0.3~0.7) were diluted into fresh medium with high-dose or no L-ara. As shown in Supplementary Fig. 3, GFP in all the samples showed a decline after dilution, consistent with the results of the stationary phase cells (Fig. 2b). Similar phenomena were also observed in the LuxR self-activation circuit (Supplementary Fig. 4). To investigate whether the dilution frequency contributes to memory loss, we studied GFP dynamics after dilution of 'ON' cells every 3 or 6 hours into fresh medium with high-dose or without L-ara. As shown in Supplementary Fig. 5, the dynamics of GFP were the same as the case without frequent dilutions (Fig. 2b) when the 'ON' cells were diluted into no L-ara fresh medium. This suggests that memory loss is not affected by the dilution frequency. When the 'ON' cells were diluted into high-dose L-ara fresh medium, the GFP level always decreased to the lowest point after each dilution (Supplementary Fig. 5). Thus, the memory loss of the SA circuit could result from dilution of gene circuit products by fast cell growth where the dilution frequency does not contribute to its memory loss.

We also found that the cell growth rate decreased while the gene expression level of the SA circuit increased (Supplementary Fig. 6), which is consistent with previous findings that synthetic circuits cause burdens to the cells and inhibit cell growth^{6,8,21,32}. Consequently, the memory loss of the SA circuit could arise from the outgrowth of ‘ON’-state cells by ‘OFF’-state cells at the population level³³. To study whether the growth rate heterogeneity among cells contributes to the memory loss here, we first conducted stochastic simulations at the single-cell level (see supplementary note for details) in three scenarios including 1) WT with both growth rate heterogeneity and growth-mediated dilution, 2) growth-mediated dilution only, and 3) growth rate heterogeneity only. As shown in Supplementary Fig. 7, while in scenario 2 the circuit lost the memory at a similar speed as it did in scenario 1 (Supplementary Fig. 7a–b and blue/red curves in Supplementary Fig. 7d), the memory loss was very slow in scenario 3 (Supplementary Fig. 7c and yellow curve in Supplementary Fig. 7d), which was not consistent with our experimental data (Fig. 2b). We then conducted an experiment by mixing various fractions of ‘OFF’ cells into ‘ON’ cells and measured the GFP dynamics to compare the speed of memory loss. As shown in Supplementary Fig. 7e–f, the curves of GFP dynamics demonstrated a similar speed of memory loss, even though the memory loss was slightly faster for the samples with more ‘OFF’ cells. Thus, we conclude that the memory loss majorly resulted from growth-mediated dilution despite the fact that growth rate heterogeneity also contributed to it.

All these data suggest the existence of a feedback loop between the synthetic gene circuit and the cell growth (Fig. 2c), in which the gene expression of circuit slows down cell growth, whereas fast cell growth dilutes the gene expression (Fig. 2c). To further understand how cell growth changes circuit behavior, we revised our mathematical model by integrating growth feedback (see supplementary note for details). We conducted a simulation to demonstrate how the SA circuit lost memory. At the populational level, a full spectrum of AraC dynamics under different levels of L-ara is shown in Fig. 2d. Initially, AraC was set at a high level but decreased very quickly to low levels, consistent with the experimental results (Fig. 2b). At the single-cell level, we developed an algorithm by considering the stochasticity from cell divisions before the system reaches the stationary phase (see supplementary note for details). Two stable steady states (SSS) and one unstable steady state (USS) can be found at the intersections of the production and degradation rates of AraC (Fig. 2e). The AraC level was set to high level in the ‘ON’ state (green circle in Fig. 2e) initially, and then decreased because of cell division-mediated dilution (blue dashed lines with yellow arrows in Fig. 2e), and later started to accumulate (solid blue lines with purple arrows in Fig. 2e) because of AraC production by the SA circuit. However, the dilution was much faster than the accumulation, and thus AraC levels decreased very quickly to a point which was below the separatrix (dash-dotted line in Fig. 2e) and converged to the ‘OFF’ state (black circle in Fig. 2e), and was maintaining in this state even after the cell growth slowed in the pre-stationary phase and stopped in the stationary phase. That is, at the early stage, the growth feedback was dominant and continuously diluted the circuit products, leading to the switching-off of the circuit. This is the underlying mechanism for the memory loss of the SA circuit and the reason why no hysteresis was found using the dilution protocol with fresh media (Figs. 1d, 2f).

For theoretical analysis, we also considered a scenario of constant growth rate to study how the strength of growth feedback affects the gene circuits (see supplementary note for details). Increasing the growth rate indeed changes the bifurcation diagram significantly (Supplementary Fig. 8a). The activation threshold of the switch increases quickly with the growth rate (Supplementary Fig. 8b). This suggests that it is unlikely to activate the system with the experiment under fast-growth conditions. Taken together, growth feedback disguises the bistable property of the SA circuit.

Decoupling growth feedback shows bistability of SA circuit

The above results showed that dilution with the fresh medium can keep cells fast-growing, but inevitably it induces the growth feedback to synthetic gene circuits, leading to memory loss. To decouple growth feedback from circuits and overcome this detrimental effect, we developed a new dilution protocol by diluting cells into the conditioned medium collected from stationary phase culture (Supplementary Fig. 9a). To test this protocol, the activated cells were first loaded into a microfluidic platform and fresh medium with or without L-ara was provided. We found that the GFP level was extinguished quickly along with several cell divisions regardless of L-ara levels (Fig. 3a-b and Supplementary Video 1–2), thereby confirming the memory loss of the SA circuit due to the growth feedback (Fig. 2b). After switching to the conditioned medium, we observed that the GFP level did not recover without L-ara (Fig. 3a and Supplementary Video 1) but elevated under high-dose L-ara (Fig. 3b and Supplementary Video 2), which is consistent with Fig. 2b. Furthermore, we measured the system dynamics under conditioned medium at the populational level. We found that cells did not divide as OD was maintained in low level (Fig. 3c and Supplementary Fig. 9b) but still had a strong ability to express the genes of the circuit since the GFP levels were well maintained during 17 hours for all L-ara concentrations (Fig. 3d and Supplementary Fig. 9c). It is noted that the maintenance of GFP is not from its slow degradation as unstable GFP variant (GFP-Iva)³⁴ with a half-life of 68 minutes is used in the circuit (Supplementary Fig. 10). This is consistent with the observed findings of a surprisingly long period of constant protein production activity in the stationary phase of bacteria³⁵. Finally, a very large range of hysteresis was revealed (Fig. 3e), indicating that the system actually functions as an irreversible bistable switch, consistent with the prediction in Fig. 1b. These data suggest that growth feedback can be decoupled under slow or non-growth conditions. To further confirm this, we diluted the activated cells into low nutrition medium M9 with either no or high-dose L-ara. The memory was maintained very well in both cases of low nutrition medium (Supplementary Fig. 11a), in contrast with the samples diluted in high nutrition medium (Supplementary Fig. 11b). Taken together, decoupling growth feedback with conditioned medium or with low-nutrient medium helps maintain circuit memory and reveals the bistability of the SA circuit.

Toggle switch is refractory to growth feedback

In order to study whether the growth feedback also affects other types of gene circuits, we tested our protocol with the toggle switch, in which two genes *TetR* and *LacI* inhibit each other. In the original work, cells were diluted into fresh medium frequently in order to maintain cells in the log growth phase²⁵. The hysteresis behavior of the toggle switch was indeed found. However, the effects of growth feedback on the toggle switch are unclear.

Thus, we studied the dynamics of the toggle switch with our protocols. At the populational level, after dilution of activated cells into fresh medium, which couples the growth feedback with the toggle switch circuit (Fig. 4a), GFP levels decreased to the minimum at 4 hours after dilution (Fig. 4b-c, Supplementary Fig. 12a-b). However, the GFP level was retrieved for all samples with various doses of inducer Anhydrotetracycline hydrochloride (aTc), indicating that the memory of the toggle switch was maintained during the fast-growth phase and can be retrieved in the slow-growth phase. Similarly, after dilution of activated cells into conditioned medium to decouple growth feedback, GFP levels were also well maintained for 17 hours (Supplementary Fig. 12c-d). The GFP maintenance is not from its slow degradation as unstable GFP variant (GFP-*laa*), which has a similar half-life as GFP-*lva*, was used in the circuit^{34,36}.

At the single-cell level with microfluidics, GFP level decreased with cell division in the fresh medium regardless of aTc doses and increased after switching to the conditioned medium both with or without aTc (Supplementary Fig. 12e-f and Supplementary Video 3-4), which is consistent with Fig. 4c. The system needed more time to recover without aTc (Supplementary Fig. 12e and Supplementary Video 3) in contrast to high dose aTc (Supplementary Fig. 12f and Supplementary Video 4). In Fig. 4d, the hysteresis curves from both conditioned medium (green curve) and fresh medium (red curve) showed the irreversibility of the toggle switch, consistent with the previous works^{25,37,38}. Thus, the toggle switch is refractory to memory loss from growth feedback.

To study how the topology differs for the response of the SA circuit and the toggle switch to growth feedback, similar simulations were done to analyze the toggle switch's behavior. First, at the populational level, no difference was found in the hysteresis curves for fast growth and no growth conditions (Supplementary Fig. 13), consistent with experimental results (Fig. 4d). At the single-cell level, the trajectory of one cell is shown to demonstrate how the system changes with several cell divisions and then recovers to the original state. As shown in the directed field for the toggle switch (Fig. 4e), two stable steady states (SSS) and one unstable steady state (USS) can be found at the intersections of the nullclines. The cell was set initially in the $\text{LacI}^{\text{High}}/\text{TetR}^{\text{Low}}$ state (solid green circle in Fig. 4e) and then moved toward the bottom-left corner (Fig. 4e, blue dashed lines with yellow arrows) due to cell division. The system tried to recover toward the top-right corner (Fig. 4e, solid blue lines with purple arrows) after each cell division. After several rounds of competition between accumulation and growth-mediated dilution, the system reached a stationary growth phase but was still in the domain where it can easily recover to the original state. We further compared the robustness of these two bistable switches to the growth-mediated effect in terms of timescale. As shown in Supplementary Fig. 14, if the timescale of the SA circuit is fast enough that it has a chance to recover to the original state after each cell division, it maintains its memory and is robust to cell growth (Supplementary Fig. 14a). That is, the SA circuit can maintain its memory theoretically, although it is highly impossible to build such a gene circuit with super-fast dynamics since transcription and translation always take time for any gene circuits. The toggle switch gene circuit is more robust in general if the timescales of LacI and TetR are balanced (Supplementary Fig. 14b). If the timescales of two genes are not well balanced with relatively slow TetR timescale, the system is still robust to the cell division (Supplementary Fig. 14c), while it could be sensitive to cell division if the LacI

timescale is significantly slow (Supplementary Fig. 14d). That is, the toggle switch maintains its memory in a much broader timescale range than the SA circuit. Taken together, the toggle switch circuit is more robust in general to the growth-mediated dilution than the SA circuit.

The major differences between the SA circuit and toggle switch are the gene promoters used in the circuits. The promoter p_{BAD} in the SA circuit is positively regulated by AraC, while promoter p_{Tet} in the toggle switch is negatively regulated by TetR. Given that the activity of promoter p_{BAD} directly depends on AraC concentration, the dilution of AraC significantly decreases its production rate in the SA circuit. While the activity of promoter p_{Tet} inversely depends on TetR concentration, the dilution of TetR does not decrease the relative production rates of the two genes in the circuit and thus leads to robust memory (Supplementary Fig. 15). These differences between the toggle switch and SA circuit are also reflected in the directions of the dilution (dashed lines with the yellow arrows in Fig. 2e and Fig. 4e). The dilution direction is more parallel to the separatrix for the toggle switch (dash-dotted line in Fig. 4e), while it is perpendicular to the separatrix for the SA circuit (dash-dotted line in Fig. 2e). This is the reason why the system has crossed the separatrix after two cell divisions for the SA circuit, while it still has not crossed the separatrix after four cell divisions for the toggle switch. In summary, the network topology of the toggle switch makes it robust to growth feedback.

DISCUSSION

It is still a big challenge to build large-sized synthetic gene circuits since oftentimes circuits do not function as expected once they are assembled. One fundamental reason is that multiple factors of circuit-host interactions, such as metabolic burden, cell growth feedback, and resource competition, are often neglected when building and testing gene circuits because of the assumption that the circuits are orthogonal to the host background. However, we know that physiological links from host to gene circuits create a hidden regulatory layer, which often perturbs the expected functions of gene circuits. In addition, it is difficult to predict how these hidden interactions affect circuit functions and how we can minimize unfavorable effects. Our data suggest that the circuit-host interaction mediated by growth feedback may disguise the true behavior of gene circuits. Most importantly, the interference depends on the network topology of gene circuits. While the SA circuit is sensitive to growth feedback and loses its memory easily, the toggle switch circuit is robust to growth feedback and can maintain its memory very well even though some decline has been found due to fast cell growth. In retrospect, this results from different dependencies of simple negative and positive regulations on growth rate⁸. The expression of target gene increases with the growth rate for a negative regulation but decreases for a positive regulation⁸. Given that most synthetic gene circuits are composed of simple negative and positive regulations, the circuit-host interactions affect each link differently and thus can significantly change gene circuits functions. Furthermore, it will be interesting to study how the noise associated with growth-related fluctuations in global gene expression affects the behavior of the circuits given that the noise level is coupled with the growth rate³⁹. The analysis of input-associated Signed Activation Time (iSAT) can be used in designing robust switches^{40,41}.

Here, we found that growth feedback has an adverse effect on the functions of some gene circuits as the memory can be lost due to fast cell growth. Previously, it has also been found that growth feedback can lend new properties to other gene circuits. A constitutively expressed antibiotic resistance gene, for example, shows innate growth bistability given that the expression of the resistance gene is growth-dependent and the cell growth is modulated by translation-targeting antibiotics²³. It is also reported that growth feedback makes some other circuit systems more cooperative^{8,21}. A non-cooperative circuit, autoregulation of T7 RNA polymerase, was found to generate bistability unexpectedly²¹. The underlying mechanism is that the nonlinear dilution of T7 RNA polymerase induced by growth feedback enhances overall effective cooperativity. Our results are consistent with this work, as an increase in growth rate indeed expands the bistable range (Supplementary Fig. 8). In the case of the autoregulation of T7 RNA polymerase, the circuit itself is not bistable, but the nonlinear dilution introduced by growth feedback increases the circuit ultrasensitivity and makes it bistable. In the case of the SA circuit here, it is bistable when growth feedback is decoupled. However, under the conditions of constant growth rate with frequent dilution into the fresh medium, the activation threshold increases so quickly that the switch's activation is infeasible in the biologically reasonable range. Thus, the effect of interactions between the circuit and the host is double-edged. While they endow new properties to some gene circuits, they impair or disguise the desired behaviors of others. Controlling strategies should be developed for the latter case. In this paper, we present a strategy by controlling the growth rate to minimize the effects of growth feedback on memory circuits. We found that conditioned medium from the stationary phase or fresh medium with minimal nutrients can be used to slow down the growth rate and thus maintain the memory of the circuits. This is also consistent with previous work that a surprisingly long period of constant protein production activity during the stationary phase of bacteria was reported³⁵.

We demonstrated how the growth feedback affects the memory maintenance of two memory gene circuits and the underlying mechanism of how the SA circuit is susceptible to growth feedback, while the toggle switch is robust. The primary factor is the perturbed concentrations of transcription activators and repressors due to cell growth, which cause the promoter activity changes of the circuits. Our results imply that the changes in gene activity during the fast cell growth phase due to the resource relocation strategy of cells during their division. That is, resources such as ATP, as well as transcriptional and translational machinery components, are biased towards cell-cell-driven changes⁴². One strategy to control this uncertainty is to integrate the synthetic gene circuits into the genome of the cell⁴³. Another method is to manipulate the size of resource pools^{44,45}. Orthogonal ribosome pools or orthogonal DNA replication systems have been used to alleviate the effect of resource competition and gene coupling⁴⁶⁻⁴⁸. Insulation-based engineering strategies have shown to improve the resolution of the genetic circuit⁴⁹. Future work is needed to further understand mechanisms of how circuit-host interactions affect gene circuits and to develop corresponding control strategies for robust gene circuits.

Methods

Strains, media and chemicals

E. coli DH10B (Invitrogen, USA) was used for all the cloning construction experiments. Measurement of the self-activated circuit was performed in *E. coli* K-12 MG1655 *lacI araCBAD* as described in²⁸. Measurement of the toggle switch was performed with *E. coli* K-12 MG1655 *lacI* as described in³⁷. Cells were grown in 5ml or 15ml tubes with 220 rotations per minute at 37 °C in Luria-Bertani broth (LB broth) with 100µg/ml chloramphenicol or 50 µg/ml kanamycin. L-(+)-Arabinose (L-ara, Sigma-Aldrich) and Anhydrotetracycline hydrochloride (aTc, Abcam) were dissolved in ddH₂O and later diluted to appropriate working solution.

Plasmids construction

The AraC self-activation circuit was constructed into either a pSB1C3 (high copy number, used for flow cytometry and plate reader analysis) or pSB3K3 (medium copy number, used for microfluidics) backbone according to the standard molecular cloning protocols using the standardized BioBricks parts from the iGEM Registry (www.parts.igem.org). The LuxR self-activation circuit was constructed into a pSB1C3 backbone. The *araC* gene was amplified by PCR using the BioBrick part BBa_C0080 as the template to have the lva-tag removed. The primers used were forward 5'-ctggaattcggcggccttctagatggctgaagcgcaaatgac-3' and reverse 5'-ggactgcagcggccgctactagtagttattatgacaactgacggctacatc-3'. The BioBricks used were BBa_B0034 (ribosome binding site, RBS), BBa_K206000 (pBAD), BBa_K145015 (gfp with lva-tag), BBA_B0015 (transcriptional terminator), and BBa_C0062 (luxR). The sequence of pLux is 5'-acctgtaggatcgtacagggttacgaagaaaatggtttgttatagtcgaataaa-3'. pLux was amplified by PCR using the BioBrick part BBa_R0062 as template. The primers used were forward 5'-gcttctagagacctgtaggatcgtacagggttacgaagaaaatggtttgttatag-3' and reverse 5'-ggactgcagcggccgctactagtagttatttcgactataacaaccattttc-3'. Detailed characterization of pLux can be found on website http://parts.igem.org/Part:BBa_R0062. All parts were firstly restriction digested using desired combinations of two FastDigest restriction enzymes chosen from EcoRI, XbaI, SpeI and PstI (Thermo Fisher) and separated by gel electrophoresis, and then purified using GelElute Gel Extraction Kit (Sigma-Aldrich) followed by ligation using T4 DNA ligase (New England BioLabs). Then the ligation products were transformed into *E. coli* strain DH10B and later the positive colonies were screened. Finally, the plasmids were extracted using GenElute Plasmids Miniprep Kit (Sigma-Aldrich) and verified by sequencing. The operons constituting the self-activation circuits were constructed monocistronically. The plasmid of the toggle switch was kindly provided by Dr. James Collins as described in^{37,38}.

Hysteresis experiment

Hysteresis experiment using conditioned medium: On day one, plasmids carrying the self-activation circuit were transformed into *E. coli* K-12 MG1655 *lacI araCBAD*. The transformants were then spread onto a LB agar plate with 100µg/ml chloramphenicol and were grown at 37°C overnight. In the morning of day two, one colony was inoculated into 200µl LB and was grown in a 5ml culture tube on a shaker for about 6 hours to reach

stationary phase. 4 μ l of the cells were then inoculated into in 4ml LB broth and were grown on a shaker at 37°C overnight using 15ml culture tubes with or without induction. For the induction of the self-activation circuit, 2.5*10⁻³% L-arabinose (L-ara) was added to the growth medium at the beginning of the experiment. An identical culture without arabinose was grown in parallel. In the morning on day three, the cells had reached the stationary phase, and the cultures were centrifuged (2000g*5min) and supernatant from the parallel culture without L-ara was sterile-filtered and was used as the conditioned medium. For flow cytometry and plate reader analysis, the pellet from L-ara containing culture was first washed twice with conditioned medium without L-ara; then the resuspended cells were diluted 100 fold into culture tubes containing 1ml conditioned medium with different concentrations of L-ara added (OD of the cells was around 0.02 measured in 200 μ l volume by plate reader). Finally, the cells were incubated in the shaker and measured at indicated time points for flow cytometry, or loaded onto a 96-well plate for plate reader analysis. Hysteresis experiment using the conditioned medium for the toggle switch was performed the same way with the induction switched to aTc.

Hysteresis experiment using fresh medium: On day one, plasmids carrying the self-activation circuit were transformed into E. coli K-12 MG1655 lacI araCBAD. The transformants were then spread onto a LB agar plate with 100 μ g/ml chloramphenicol and were grown at 37°C overnight. In the morning of day two, one colony was inoculated into 200 μ l LB and was grown in a 5ml culture tube on a shaker for about 6 hours to reach the stationary phase. 4 μ l of the cells were then inoculated into in 4ml LB broth and were grown on a shaker at 37°C overnight using 15ml culture tubes with or without induction. For the induction of the self-activation circuit, 2.5*10⁻³% L-arabinose (L-ara) was added to the growth medium at the beginning of the experiment. In the morning of day three, the cultures were centrifuged (2000g*5min) and the pellet was first washed twice with warm LB without L-ara; then the resuspended cells were diluted 100 fold into culture tubes containing 1ml fresh medium with different concentrations of L-ara added (OD of the cells was around 0.02 measured in 200 μ l volume by plate reader). Finally, the cells were incubated in the shaker and measured at indicated time points for flow cytometry, or loaded onto a 96-well plate for plate reader analysis. Hysteresis experiment using fresh medium for the toggle switch was performed the same way with the induction switched to aTc.

Flow cytometry

All samples were analyzed using Accuri C6 flow cytometer (Becton Dickinson) with excitation/emission filters 480nm/530nm (FL1-A) for GFP detection at indicated time points. 10,000 events were recorded for each sample. At least three replicated tests were performed for each experiment. Data files were analyzed with MATLAB (MathWorks).

Dynamic analysis performed by Plate Reader

Synergy H1 Hybrid Reader from BioTek was used to perform the dynamic analysis. 200 μ l of culture was loaded into each well of the 96-well plate. LB broth without cells was used as a blank. The plate was incubated at 37°C with orbital shaking at the frequency of 807cpm (circles per minute). Cell density (optical density, OD) of the culture was measured by

absorbance at 600nm; GFP was detected by excitation/emission at 485nm/515nm. All the measurements were taken at 15- or 30-minutes intervals.

Estimation of the GFP-Iva half-life

Plasmids carrying circuit shown in Fig. 1a were transformed into *E. coli* K-12 MG1655 *lacI araCBAD*. The transformants were then grown on a LB agar plate with 100µg/ml chloramphenicol overnight at 37°C. In the afternoon of the second day, one colony was inoculated into 5ml LB supplemented with 100µg/ml chloramphenicol in a 15ml culture and was grown overnight with 220 rotations per minute at 37 °C. In the morning of the third day, 20µl of the overnight culture was firstly inoculated into 2ml LB with 100µg/ml chloramphenicol in a 15ml tube and was grown to late exponential phase (OD~1.0; OD was measured by plate reader with 200µl culture in one well on the 96-well plate). Then the cells were induced with 2.5*10⁻³% L-ara for 45 min. Later, cells were washed with conditioned medium collected from overnight uninduced culture carrying the same circuit for three times and were resuspended in conditioned medium without L-ara. Last, the cell suspensions were loaded onto a 96-well plate with 200µl per well, and OD and GFP fluorescence were measured every 15 minutes by the plate reader.

Microfluidics and microscopy

On day one, plasmids carrying the self-activation circuit were transformed into *E. coli* K-12 MG1655 *lacI araCBAD*. The transformants were then spread onto a LB agar plate with 100µg/ml chloramphenicol and were grown at 37°C overnight. In the morning of the second day, one colony was inoculated into 200µl LB and were grown in a 5ml culture tube on a shaker for about 6 hours to reach the stationary phase. 4µl of the cells were then inoculated into 4ml LB broth and were grown on a shaker at 37°C overnight using 15ml culture tubes with or without induction. In the morning of the third day, the cells were centrifuged at 2000g*5min followed by resuspension into 0.5 ml fresh medium with 0.75% Tween-80 (Sigma-Aldrich) and loaded onto the device. After the cells were loaded onto the device properly, fresh media with indicated induction was supplied to the cell for 16 hours; then on day four, the cells were switched to conditioned medium with indicated induction for various amounts of time as needed. Media switching was accomplished by adjusting the relative height of syringes containing fresh or conditioned medium. Details regarding the design of the chip and setup of the device can be found in ref.⁵⁰. Phase and green fluorescent images were taken every 15 min under the magnification of 40X with Nikon Eclipse Ti inverted microscope (Nikon, Japan) equipped with an LED-based Lumencor SOLA SE. Perfect focus was obtained automatically using Nikon Elements software. Microfluidics for the toggle switch was performed the same way with the induction switched to aTc.

Mathematical modeling

Ordinary differential equation models were developed to describe and analyze the interplay between the self-activation and toggle switch circuits and the host cell growth at the population level. The stochastic simulation algorithm was developed to characterize the stochastic cell division events at the single-cell level. Details are provided in the supplementary note.

Supplementary Material

Refer to Web version on PubMed Central for supplementary material.

Acknowledgments

We thank X. Fu, T. Hong, G. Yao, J. Xing, W. Shou, and T. Hwa for valuable comments. This project was supported by the ASU School of Biological and Health Systems Engineering and NSF grant (EF-1921412) (to X.-J.T.), and NIH grant (GM106081) (to X.W.). H Goetz and J Melendez-Alvarez were also supported by the Arizona State University Dean's Fellowship.

Reference:

1. Brophy JA & Voigt CA Principles of genetic circuit design. *Nat Methods* 11, 508–520, doi:10.1038/nmeth.2926 (2014). [PubMed: 24781324]
2. Liao C, Blanchard AE & Lu T. An integrative circuit-host modelling framework for predicting synthetic gene network behaviours. *Nat Microbiol* 2, 1658–1666, doi:10.1038/s41564-017-0022-5 (2017). [PubMed: 28947816]
3. Boo A, Ellis T. & Stan G-B Host-aware synthetic biology. *Curr Opin Syst Biol* 14, 66–72, doi:10.1016/j.coisb.2019.03.001 (2019).
4. Lynch M. & Marinov GK The bioenergetic costs of a gene. *Proc Natl Acad Sci U S A* 112, 15690–15695, doi:10.1073/pnas.1514974112 (2015). [PubMed: 26575626]
5. Ceroni F. et al. Burden-driven feedback control of gene expression. *Nat Methods* 15, 387–393, doi:10.1038/nmeth.4635 (2018). [PubMed: 29578536]
6. Scott M, Gunderson CW, Mateescu EM, Zhang Z. & Hwa T. Interdependence of cell growth and gene expression: origins and consequences. *Science* 330, 1099–1102, doi:10.1126/science.1192588 (2010). [PubMed: 21097934]
7. Weisse AY, Oyarzun DA, Danos V. & Swain PS Mechanistic links between cellular trade-offs, gene expression, and growth. *Proc Natl Acad Sci U S A* 112, E1038–1047, doi:10.1073/pnas.1416533112 (2015). [PubMed: 25695966]
8. Klumpp S, Zhang Z. & Hwa T. Growth rate-dependent global effects on gene expression in bacteria. *Cell* 139, 1366–1375, doi:10.1016/j.cell.2009.12.001 (2009). [PubMed: 20064380]
9. Qian Y, Huang HH, Jimenez JI & Del Vecchio D. Resource Competition Shapes the Response of Genetic Circuits. *ACS Synth Biol* 6, 1263–1272, doi:10.1021/acssynbio.6b00361 (2017). [PubMed: 28350160]
10. Erickson DW et al. A global resource allocation strategy governs growth transition kinetics of *Escherichia coli*. *Nature* 551, 119–123, doi:10.1038/nature24299 (2017). [PubMed: 29072300]
11. Venturelli OS et al. Programming mRNA decay to modulate synthetic circuit resource allocation. *Nat Commun* 8, 15128 (2017). [PubMed: 28443619]
12. Klumpp S. & Hwa T. Growth-rate-dependent partitioning of RNA polymerases in bacteria. *Proc Natl Acad Sci U S A* 105, 20245–20250, doi:10.1073/pnas.0804953105 (2008). [PubMed: 19073937]
13. Lu TK, Khalil AS & Collins JJ Next-generation synthetic gene networks. *Nature biotechnology* 27, 1139–1150, doi:10.1038/nbt.1591 (2009).
14. Purnick PE & Weiss R. The second wave of synthetic biology: from modules to systems. *Nat Rev Mol Cell Biol* 10, 410–422, doi:10.1038/nrm2698 (2009). [PubMed: 19461664]
15. Kwok R. Five hard truths for synthetic biology. *Nature* 463, 288–290, doi:10.1038/463288a (2010). [PubMed: 20090726]
16. Purcell O, Jain B, Karr JR, Covert MW & Lu TK Towards a whole-cell modeling approach for synthetic biology. *Chaos* 23, 025112, doi:10.1063/1.4811182 (2013). [PubMed: 23822510]
17. Cardinale S. & Arkin AP Contextualizing context for synthetic biology--identifying causes of failure of synthetic biological systems. *Biotechnology journal* 7, 856–866, doi:10.1002/biot.201200085 (2012). [PubMed: 22649052]

18. Zhang C, Tsoi R. & You L. Addressing biological uncertainties in engineering gene circuits. *Integrative biology : quantitative biosciences from nano to macro* 8, 456–464, doi:10.1039/c5ib00275c (2016). [PubMed: 26674800]
19. Arkin AP A wise consistency: engineering biology for conformity, reliability, predictability. *Curr Opin Chem Biol* 17, 893–901, doi:10.1016/j.cbpa.2013.09.012 (2013). [PubMed: 24268562]
20. Klumpp S. & Hwa T. Bacterial growth: global effects on gene expression, growth feedback and proteome partition. *Curr Opin Biotechnol* 28, 96–102, doi:10.1016/j.copbio.2014.01.001 (2014). [PubMed: 24495512]
21. Tan C, Marguet P. & You L. Emergent bistability by a growth-modulating positive feedback circuit. *Nat Chem Biol* 5, 842–848, doi:10.1038/nchembio.218 (2009). [PubMed: 19801994]
22. Nevozhay D, Adams RM, Van Itallie E, Bennett MR & Balazsi G. Mapping the environmental fitness landscape of a synthetic gene circuit. *PLoS Comput Biol* 8, e1002480, doi:10.1371/journal.pcbi.1002480 (2012). [PubMed: 22511863]
23. Deris JB et al. The innate growth bistability and fitness landscapes of antibiotic-resistant bacteria. *Science* 342, 1237435, doi:10.1126/science.1237435 (2013). [PubMed: 24288338]
24. Feng J, Kessler DA, Ben-Jacob E. & Levine H. Growth feedback as a basis for persister bistability. *Proc Natl Acad Sci U S A* 111, 544–549, doi:10.1073/pnas.1320396110 (2014). [PubMed: 24344277]
25. Gardner TS, Cantor CR & Collins JJ Construction of a genetic toggle switch in *Escherichia coli*. *Nature* 403, 339–342, doi:10.1038/35002131 (2000). [PubMed: 10659857]
26. Lou C. et al. Synthesizing a novel genetic sequential logic circuit: a push-on push-off switch. *Mol Syst Biol* 6, 350–350, doi:10.1038/msb.2010.2 (2010). [PubMed: 20212522]
27. Isaacs FJ, Hasty J, Cantor CR & Collins JJ Prediction and measurement of an autoregulatory genetic module. *Proc Natl Acad Sci U S A* 100, 7714–7719, doi:10.1073/pnas.1332628100 (2003). [PubMed: 12808135]
28. Wu F, Su RQ, Lai YC & Wang X. Engineering of a synthetic quadrastable gene network to approach Waddington landscape and cell fate determination. *Elife* 6, e23702, doi:10.7554/eLife.23702 (2017). [PubMed: 28397688]
29. Zeng W. et al. Rational Design of an Ultrasensitive Quorum-Sensing Switch. *ACS Synth Biol* 6, 1445–1452, doi:10.1021/acssynbio.6b00367 (2017). [PubMed: 28437094]
30. Li T. et al. Engineering of a genetic circuit with regulatable multistability. *Integrative biology : quantitative biosciences from nano to macro* 10, 474–482, doi:10.1039/c8ib00030a (2018). [PubMed: 30039143]
31. Wu F, Menn DJ & Wang X. Quorum-sensing crosstalk-driven synthetic circuits: from unimodality to trimodality. *Chem Biol* 21, 1629–1638, doi:10.1016/j.chembiol.2014.10.008 (2014). [PubMed: 25455858]
32. Dong H, Nilsson L. & Kurland CG Gratuitous overexpression of genes in *Escherichia coli* leads to growth inhibition and ribosome destruction. *J Bacteriol* 177, 1497–1504, doi:10.1128/jb.177.6.1497-1504.1995 (1995). [PubMed: 7883706]
33. Blanchard AE, Liao C. & Lu T. Circuit-Host Coupling Induces Multifaceted Behavioral Modulations of a Gene Switch. *Biophys J* 114, 737–746, doi:10.1016/j.bpj.2017.12.010 (2018). [PubMed: 29414718]
34. Andersen JB et al. New unstable variants of green fluorescent protein for studies of transient gene expression in bacteria. *Appl Environ Microbiol* 64, 2240–2246 (1998). [PubMed: 9603842]
35. Gefen O, Fridman O, Ronin I. & Balaban NQ Direct observation of single stationary-phase bacteria reveals a surprisingly long period of constant protein production activity. *Proc Natl Acad Sci U S A* 111, 556–561, doi:10.1073/pnas.1314114111 (2014). [PubMed: 24344288]
36. Litcofsky KD, Afeyan RB, Krom RJ, Khalil AS & Collins JJ Iterative plug-and-play methodology for constructing and modifying synthetic gene networks. *Nat Methods* 9, 1077–1080, doi:10.1038/nmeth.2205 (2012). [PubMed: 23042452]
37. Menn D, Sochor P, Goetz H, Tian XJ & Wang X. Intracellular Noise Level Determines Ratio Control Strategy Confined by Speed-Accuracy Trade-off. *ACS Synth Biol* 8, 1352–1360, doi:10.1021/acssynbio.9b00030 (2019). [PubMed: 31083890]

38. Wu M. et al. Engineering of regulated stochastic cell fate determination. *Proc Natl Acad Sci U S A* 110, 10610–10615, doi:10.1073/pnas.1305423110 (2013). [PubMed: 23754391]
39. Keren L. et al. Noise in gene expression is coupled to growth rate. *Genome Research* 25, 1893–1902, doi:10.1101/gr.191635.115 (2015). [PubMed: 26355006]
40. Wang L, Xin J. & Nie Q. A critical quantity for noise attenuation in feedback systems. *PLoS Comput Biol* 6, e1000764, doi:10.1371/journal.pcbi.1000764 (2010). [PubMed: 20442870]
41. Chen M, Wang L, Liu CC & Nie Q. Noise attenuation in the ON and OFF states of biological switches. *ACS Synth Biol* 2, 587–593, doi:10.1021/sb400044g (2013). [PubMed: 23768065]
42. Slager J. & Veening JW Hard-Wired Control of Bacterial Processes by Chromosomal Gene Location. *Trends Microbiol* 24, 788–800, doi:10.1016/j.tim.2016.06.003 (2016). [PubMed: 27364121]
43. Moon TS, Lou C, Tamsir A, Stanton BC & Voigt CA Genetic programs constructed from layered logic gates in single cells. *Nature* 491, 249 (2012). [PubMed: 23041931]
44. Zhong Z, Ravikumar A. & Liu CC Tunable Expression Systems for Orthogonal DNA Replication. *ACS Synth Biol* 7, 2930–2934, doi:10.1021/acssynbio.8b00400 (2018). [PubMed: 30408954]
45. Liu CC, Jewett MC, Chin JW & Voigt CA Toward an orthogonal central dogma. *Nat Chem Biol* 14, 103–106, doi:10.1038/nchembio.2554 (2018). [PubMed: 29337969]
46. Arzumanyan GA, Gabriel KN, Ravikumar A, Javanpour AA & Liu CC Mutually Orthogonal DNA Replication Systems In Vivo. *ACS Synth Biol* 7, 1722–1729, doi:10.1021/acssynbio.8b00195 (2018). [PubMed: 29969238]
47. Darlington APS, Kim J, Jimenez JI & Bates DG Dynamic allocation of orthogonal ribosomes facilitates uncoupling of co-expressed genes. *Nat Commun* 9, 695, doi:10.1038/s41467-018-02898-6 (2018). [PubMed: 29449554]
48. An W. & Chin JW Synthesis of orthogonal transcription-translation networks. *Proc Natl Acad Sci U S A* 106, 8477–8482, doi:10.1073/pnas.0900267106 (2009). [PubMed: 19443689]
49. Zong Y. et al. Insulated transcriptional elements enable precise design of genetic circuits. *Nat Commun* 8, 52, doi:10.1038/s41467-017-00063-z (2017). [PubMed: 28674389]
50. Ferry MS, Razinkov IA & Hasty J. in *Methods Enzymol* Vol. 497 (ed Voigt Chris) 295–372 (Academic Press, 2011). [PubMed: 21601093]

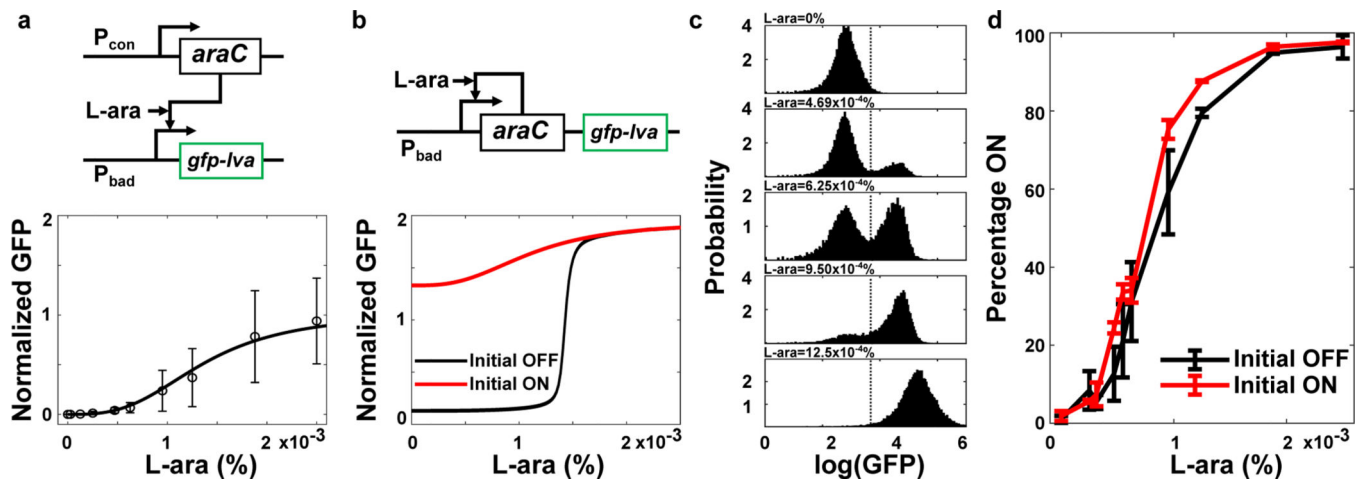


Figure 1. Theoretical analysis reveals bistability, but experimental data shows no hysteresis.
a, Parameter fitting the dose-response curve of the promoter (P_{BAD}) shows ultrasensitivity. The results showed mean \pm s.d. (n=6). Unstable GFP variant (GFP-lva) is used as the reporter.
b, Mathematical model predicts bistability from the SA circuit with P_{BAD} promoter. **c**, Steady-state distribution of GFP after 17 hours induction of various doses of L-ara with the initial state 'OFF' shows two distinct states (separated by the dash lines), 'ON' and 'OFF'.
d, The steady-state fraction of 'ON' cells after 17 hours induction of L-ara with the initial state 'OFF' (blue curve) or 'ON' (Red curve) shows no hysteresis. The 'ON' cells were pretreated with high-dose of L-ara ($2.5 \times 10^{-3}\%$). Data displayed as mean \pm s.d. (n=3).

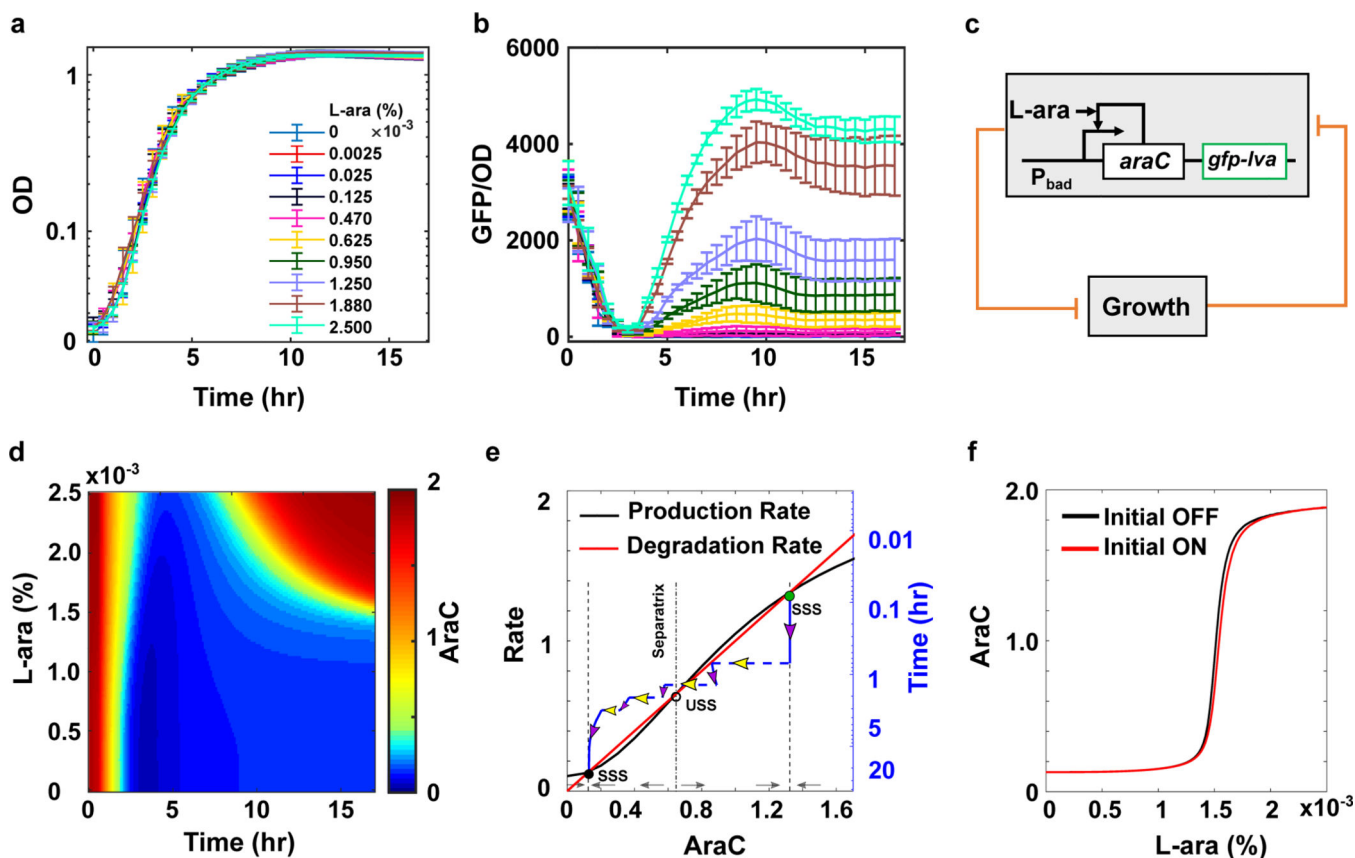


Figure 2. Growth-mediated feedback disguises the bistability of the SA circuit.

a-b, Dynamics of growth (Optical Density, OD) (a) and GFP/OD (b) after 1:100 dilution of ‘ON’ cells into fresh medium with various doses of L-ara. Data indicate mean \pm s.d. (n=3). **c**, Diagram of coupling gene circuit with cell growth. The mathematical model is revised based on this diagram. **d**, Simulation with revised mathematical model shows AraC level as a function of time and L-ara dose. The system was set to ‘ON’ state initially. **e**, The process of memory loss of the SA circuit. Simulated trajectory (blue lines) of one cell is shown on the rate-balance plot of AraC. Two stable steady states (SSS, solid circles) and one unstable steady state (USS, open circle) are shown at the intersection of the production rate curve (green) and degradation curve (red). The system was set to the ‘ON’ state initially (solid green circle) and L-ara was set to 0. Four cell division events were considered in simulation (dashed line with yellow arrow). The separatrix (dash-dotted line) determines whether the system goes to ‘ON’ or ‘OFF’ states directed by the gray arrows. The rate-balance plot is based on the model without growth feedback. **f**, Simulation confirms that the bistable range of the SA circuit is significantly reduced when coupled with growth feedback.

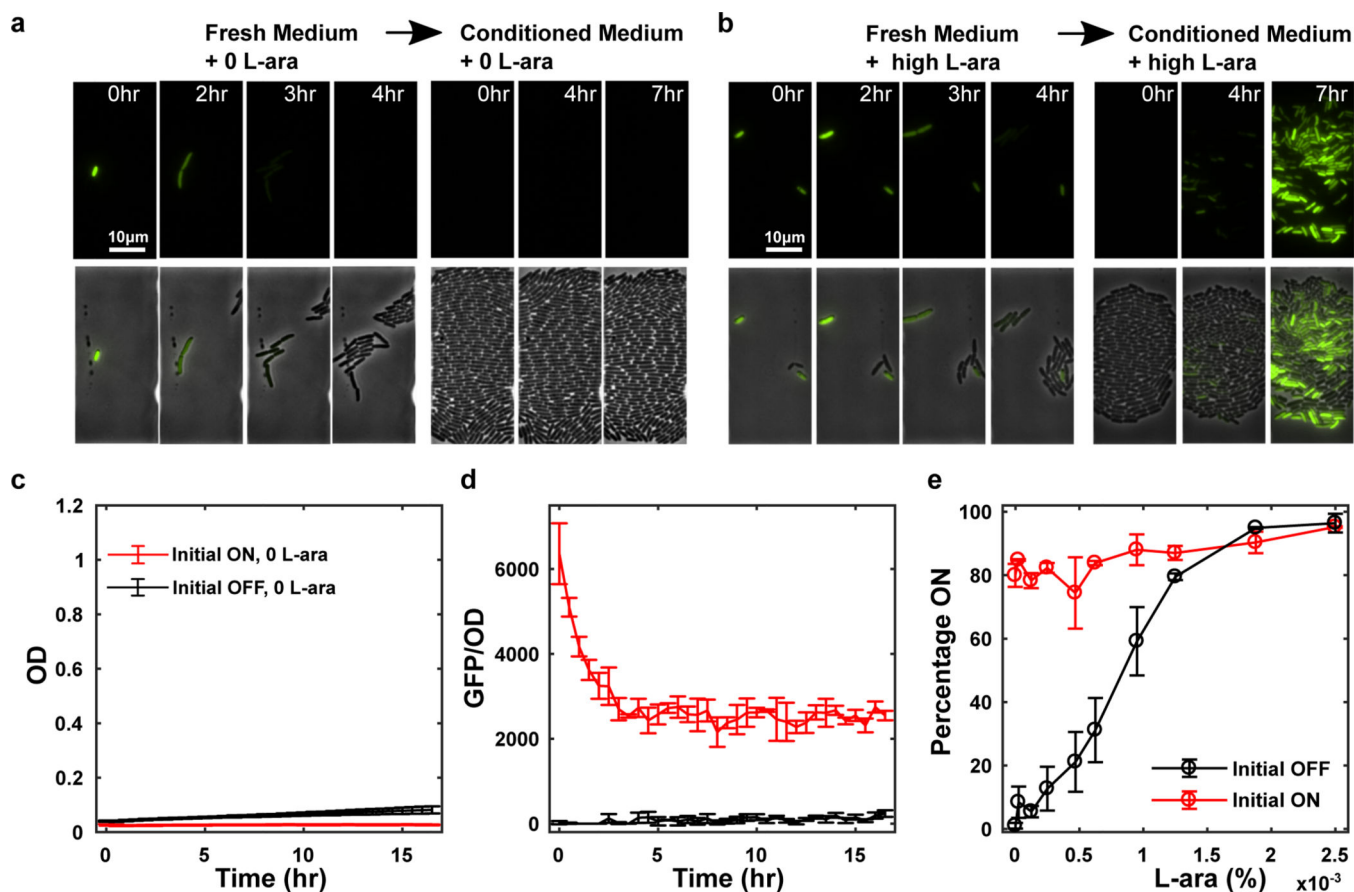


Figure 3. Decoupling of growth feedback reveals the bistability of the SA circuit.

a-b, Time-lapse imaging of GFP (and brightfield overlay) in the SA circuit showed that it switches off after several rounds of cell divisions with fast growth in fresh medium and then did not recover in the conditioned medium without inducer (a) but recovered with high-dose L-ara (b). Representative results from three replicates are shown. **c-d**, The dynamics of growth (c) and GFP (d) after 1:100 dilution of ‘ON’ cells into the conditioned medium without L-ara. Negative control (blue line) was the ‘OFF’ cells grown in conditioned medium with no L-ara. **e**, Hysteresis curves obtained using the new protocol by diluting ‘ON’ cells into the conditioned medium with various doses of L-ara. Data indicate mean \pm s.d. (n=3).

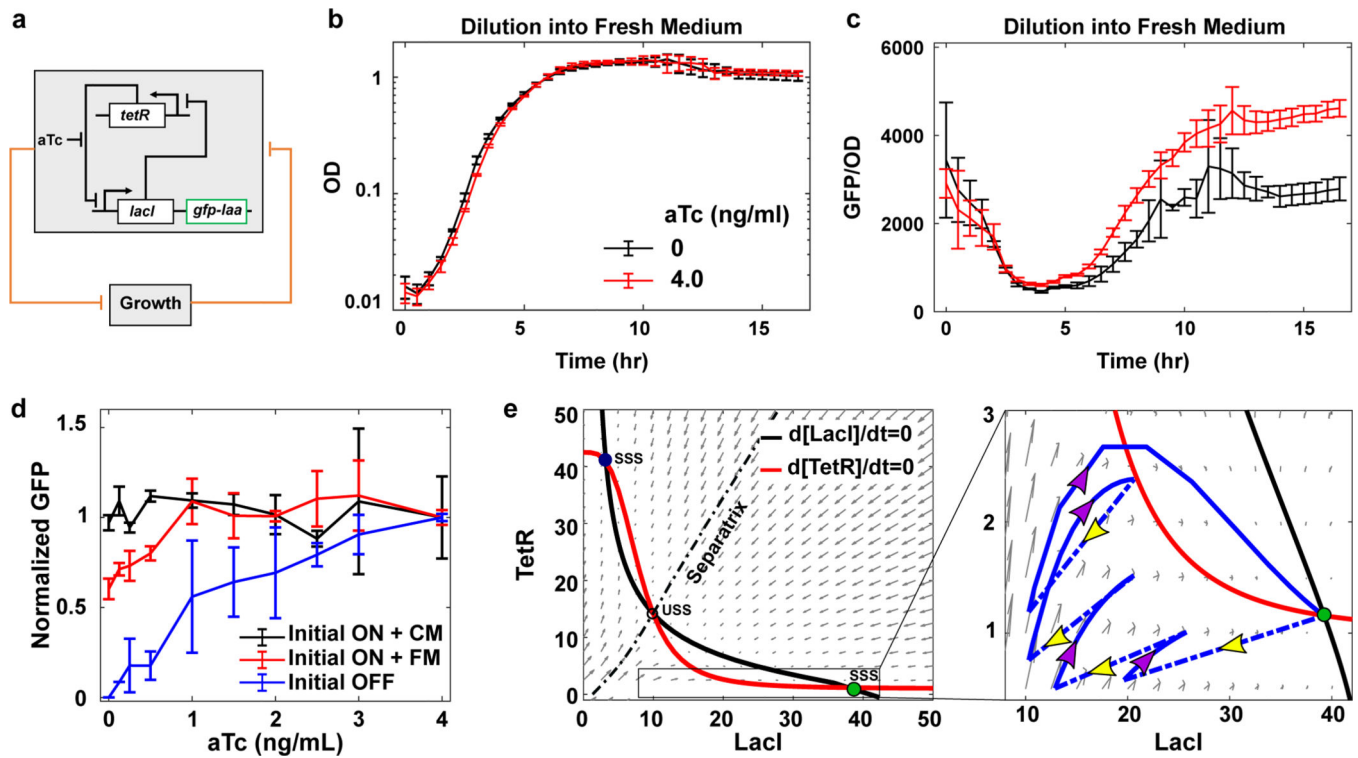


Figure 4. The toggle switch is refractory to memory loss from the growth-mediated feedback. **a**, Diagram of the toggle switch circuit coupled with growth feedback. Unstable GFP variant (GFP-*laa*) is used as the reporter. **b-c**, Dynamics of OD and GFP/OD after 1:100 dilution of ‘ON’ cells into fresh medium with high-dose or without inducer aTc. **d**, Hysteresis curves with conditioned medium (CM, green curve) and fresh medium (FM, red curve). GFP level was normalized to the level at the highest aTc. **e**, Simulated trajectory (blue lines) of one cell is shown in the direction field of LacI/TetR. Four cell division events were considered (indicated by dashed lines with yellow arrows in the enlarged box area). Two stable steady states (SSS, solid circles) and one unstable steady state (USS, open circle) are shown at the intersection of nullclines (green and red curves). The system was set to the ‘ON’ state initially (solid green circle) and aTc was set to 0. The separatrix (dash-dotted line) determines whether the system goes to the ‘ON’ or ‘OFF’ state directed by the gray arrows. The nullcline curves were based on the model without growth feedback. Data indicate mean \pm s.d. (n=3).